Electronic Supplementary Material (ESI) for Dalton Transactions.
This journal is © The Royal Society of Chemistry 2021

Supplementary Material

Improving the single-molecule magnet properties of two pentagonal bipyramidal Dy^{3+} compounds by the introduction of both electron-withdrawing and -donating groups

Li Zhu,[†,¶] Yubao Dong,[†,¶] Bing Yin,[‡] Pengtao Ma[§] and Dongfeng Li*[†]

[†] Key Laboratory of Pesticide & Chemical Biology, Ministry of Education, College of Chemistry, Central China Normal University, Wuhan 430079, P. R. China.

[‡] Key Laboratory of Synthetic and Natural Functional Molecule of the Ministry of Education, College of Chemistry and Materials Science, Northwest University, Xi'an 710127, P. R. China.

[§]Henan Key Laboratory of Polyoxometalate Chemistry, College of Chemistry and Chemical Engineering, Henan University, Kaifeng, Henan 475004, P. R. China.

*E-mail: dfli@mail.ccnu.edu.cn, rayinyin@nwu.edu.cn

Content

1. Physical Measurements

Elemental analyses for C, H, and N microanalyses were carried out with a Perkin-Elmer 240Q elemental analyzer. The FT-IR spectra were recorded from KBr pellets in the range 4000-400 cm^{-1} on a Bruker Tensor 27 spectrophotometer. The molecular weight was operated with a Finnigan LCQ Advantage MAX (m/z: 50-2000) under the positive ion mode with the ESI source on Shimadzu GCMS-QP2020 GC/MS mass spectrometer. The ^{1}H spectra were recorded on a Bruker 400 MHz. Powder X-ray diffraction patterns (PXRD) were measured at 296 K on a Bruker AXS D8 Advance powder diffractometer at 40 kV, 40 mA for Cu-Kα (λ = 1.5406 Å), with a scan speed of 0.2 s/step and a step size of 0.01° in 2θ. Using single crystal X-ray diffraction data to calculate the simulated PXRD patterns and process it by the free Mercury v1.4 program provided by the Cambridge Crystallographic Data Center. An accurate yttrium/dysprosium ratio was measured using the inductively coupled plasma (ICP) optical emission spectra on a Prodigy 7 spectrometry.

X-ray Crystallography

Appropriate single crystals of **1** and **2** were selected from the mother liquor. The single-crystal X-ray diffraction experiment data was performed at 296 K on a Bruker APEX II CCD diffractometer equipped with a charge-coupled device (CCD) area detector using graphite-monochromated Mo Kα radiation (λ = 0.71073 Å). The unit-cell parameters were generally determined using APEXII program. The data were integrated with the SAINT program. The absorption correction based on multi-scan was applied using SADABS (IC, 2019, 58, 15330). The structures of all compounds were solved by the direct methods in SHELXTL and refined with a full-matrix least-squares method on F^2 (SHELXL-2014) using the Olex-2 software. Non-hydrogen atoms were successfully refined with anisotropic displacement parameters. All the hydrogen atoms of organic ligands were recommended in idealized positions and refined with a fixed geometry with respect to their carrier atoms. All crystal data and the final structural refinement parameters for the studied compounds **1**–**4** are listed in Table S1, and the important bond lengths and bond angles are given in Table S2.

Magnetic Measurements

The polycrystalline samples were isolated via filtration from the mother liquor and left to air-dry on a filter paper and measured. Magnetic susceptibility measurements were performed on a Quantum Design MPMS-XL-5 SQUID magnetometer during cooling. The $\chi_M T$ values were corrected by the diamagnetic part calculated by Pascal′s constant.

Ab Initio Computations

Complete active space self-consistent field (CASSCF) calculations with MOLCAS 8.0 program package were carried out on the crystallographically determined coordinates of compounds **1** and **2** to determine the relative energies of the Kramers' doublets in the $^6H_{15/2}$ ground state of the Dy^{3+} ions. The SINGLE_ANISO module was used to obtain the *g*-tensors, transition magnetic moments and other parameters characterizing the magnetic anisotropy. The original geometry for theoretical calculations was drawn from the single crystal X-ray structural determinations.

2.Syntheses of the ligands

N,N′-bis-(5-methyl-2-hydroxybenzyl)ethylene-diamine (H_2bmben). The solution of 5-methylsalicylaldehyde (40 mmol, 5.45 g) in 40 mL ethanol. The ethanol (40 mL) solution of ethylenediamine (21.6 mmol, 1.30 g) was slowly added to the ethylenediamine solution and then yellow precipitate was formed. The mixing was stirred at room temperature for 1.5 h and then putted it in ice water for 15 min. $NaBH_4$ (54 mmol, 2.02 g) was added to the mixture. The reaction was stirred at room temperature for 2 h and white precipitate were formed. The precipitate was filtered, washed with water, and then dried in vacuo and 6.31 g white powder was obtained. The yield was 97.3%. ESI-MS: m/z = 301.15 [M-H^+], ^{1}H NMR (400 MHz, $CDCl_3$): δ = 6.99-6.95 (m, 2H), 6.78 (s, 2H), 6.73 (d, J = 8.2 Hz, 2H), 3.95 (s, 4H), 2.82 (s, 4H), 2.24 (s, 6H).

N,N′-bis-(5-methyl-2-hydroxybenzyl)-N,N′-bis(5-fluoro-2-methylpyridyl)ethylene diamine (H_2bmbpen-F). A solution of 2-(bromomethyl)-5-fluoropyridine hydrobromide (2.79 g, 10 mmol) dissolved in water (30 mL), and added the 2 M NaOH, to adjust the pH to 8-9. A solution of H_2bmben (1.5 g, 5 mmol) in 2 M NaOH (12 mL) was added with stirring. The mixing reaction was then heated to 85 °C and NaOH (2 M) was added during over a period of 3 h in small batches so that the pH never exceeded 10. The red solution was cooled and extracted with chloroform (10 × 70 mL). The organic phase was dried over anhydrous Na_2SO_4. The solvent was removed under vacuum. a red residue was obtained. The crude was purified by Chromatography on silica gel (DCM/PE = 1: 4, v/v) to yield the product as a white solid, 1.23 g, yield: 47.4 %. ESI-MS: m/z = 519.2 [M-H^+], ^{1}H NMR (400 MHz, $CDCl_3$): δ = 8.38 (d, J = 2.8 Hz, 2H), 7.33 (td, J = 8.4. 2.9 Hz, 2H), 7.18 (dd, J = 8.6, 4.3 Hz, 2H), 6.95 (d, J = 8.1 Hz, 2H), 6.71-6.68 (m, 4H), 3.70 (s, 4H), 3.64 (s, 4H), 2.72 (s, 4H), 2.22 (s, 6H). IR (KBr pellet, cm^{-1}): 3057 (w), 2925 (m), 2829 (w), 1581 (m), 1489 (s), 1390 (m), 1253 (s), 1109 (m), 1062 (m), 962 (m), 908 (m), 821 (s), 763 (m), 651 (w), 570 (w), 509 (w), 453 (w).

3.Single crystal X-ray crystallographic data

Table S1a. Crystal data and structure refinement for compounds **1** and **2**.

Compound	**1**	**2**
Formula	$C_{30}H_{30}ClDyF_2N_4O_2$	$C_{30}H_{30}BrDyF_2N_4O_2$
Formula weight	714.53	758.99
Temperature / K	296	296
Crystal system	Monoclinic	Monoclinic
Space group	$P2_1/n$	$P2_1/n$
a / Å	8.6403 (5)	8.6384 (3)
b / Å	18.2643 (12)	18.2435 (7)
c / Å	17.8656 (12)	17.9368 (6)
α/ °	90	90
β/ °	91.179 (2)	91.320 (1)
γ / °	90.00	90.00
V /Å^3	2818.8 (3)	2825.99 (17)
Z	4	4
F(000)	1420	1492
D_{calc} /Mg m^{-3}	1.684	1.784
Mo Kα /Å	0.71073	0.71073
μ / (mm^{-1})	2.79	4.11
R_{int}	0.047	0.052
Collected reflections	39684	31473
Unique reflections	8601	8666
Goodness-of-fit on F^2	1.09	1.1
R_1 [$I>2\sigma(I)$]^a	0.0358	0.0442
wR_2 [$I>2\sigma(I)$]^b	0.0683	0.0904
R_1, *(all data)*^{a}	0.0524	0.0702
wR_2, *(all data)*^{b}	0.0747	0.1006

$^a R_1 = \Sigma(F_o - F_c)/\Sigma F_o$. $^b wR_2 = [\Sigma w(F_o^2 - F_c^2)^2/\Sigma w(F_o^2)^2]^{1/2a}$.

Table S1b. Crystal data and structure refinement for compounds **3** and **4**.

Compound	**3**	**4**
Formula	$C_{30}H_{30}ClYF_2N_4O_2$	$C_{30}H_{30}BrYF_2N_4O_2$
Formula weight	640.94	685.40
Temperature / K	296	296
Crystal system	Monoclinic	Monoclinic
Space group	$P2_1/n$	$P2_1/n$
a / Å	8.6179 (13)	8.623 (6)
b / Å	18.254 (3)	18.225 (13)
c / Å	17.868 (3)	17.923 (13)
α/ °	90	90
β/ °	91.093 (2)	89.931 (2)
γ / °	90.00	90.00
V /Å^3	2810.4 (7)	2816 (4)
Z	4	4
F(000)	1312	1384
D_{calc} /Mg m^{-3}	1.515	1.616
Mo Kα /Å	0.71073	0.71073
μ / (mm^{-1})	2.22	3.54
R_{int}	0.044	0.241
Collected reflections	19332	19816
Unique reflections	4955	4949
Goodness-of-fit on F^2	1.02	1.01
R_1 [$I>2\sigma(I)$]^a	0.0306	0.1062
wR_2 [$I>2\sigma(I)$]^b	0.0774	0.2197
R_1, *(all data)*^{a}	0.0437	0.1716
wR_2, *(all data)*^{b}	0.0827	0.2635

$^aR_1 = \Sigma(F_o - F_c)/\Sigma F_o$. $^bwR_2 = [\Sigma w(F_o^2 - F_c^2)^2/\Sigma w(F_o^2)^2]^{1/2a}$.

Table S2. Selected bond lengths (Å) and angles (°) for compounds **1**–**2**.

1			
Bond lengths around Dy(1)			
Dy(1)–O(1)	2.156 (2)	Dy(1)–N(3)	2.602 (3)
Dy(1)–O(2)	2.166 (2)	Dy(1)–N(4)	2.560 (3)
Dy(1)–N(1)	2.591 (3)	Dy(1)–Cl(1)	2.6576 (10)
Dy(1)–N(2)	2.591 (3)		
Bond angles including Dy(1)			
O(1)–Dy(1)–O(2)	158.09 (9)	N(3)–Dy(1)–Cl(1)	146.22 (6)
O(1)–Dy(1)–Cl(1)	100.87 (7)	N(2)–Dy(1)–Cl(1)	144.49 (6)
O(1)–Dy(1)–N(3)	76.54 (8)	N(2)–Dy1–N(3)	69.29 (8)
O(1)–Dy(1)–N(2)	86.73 (9)	N(2)–Dy(1)–N(1)	64.43 (8)
O(1)–Dy(1)–N(1)	89.75 (9)	N(1)–Dy(1)–Cl(1)	80.83 (7)
O(1)–Dy(1)–N(4)	90.20 (9)	N(1)–Dy(1)–N(3)	132.30 (9)
O(2)–Dy(1)–Cl(1)	100.90 (7)	N(4)–Dy(1)–Cl(1)	81.30 (7)
O(2)–Dy(1)–N(3)	84.03 (9)	N(4)–Dy(1)–N(3)	65.14 (9)
O(2)–Dy1–N(2)	76.88 (9)	N(4)–Dy(1)–N(2)	133.74 (9)
O(2)–Dy(1)–N(1)	96.03 (9)	N(4)–Dy(1)–N(1)	161.79 (9)
O(2)–Dy(1)–N(4)	90.75 (9)		

2			
Bond lengths around Dy(1)			
Dy(1)–O(1)	2.157 (3)	Dy(1)–N(3)	2.597 (3)
Dy(1)–O(2)	2.158 (3)	Dy(1)–N(4)	2.566 (4)
Dy(1)–N(1)	2.600 (4)	Dy(1)–Br(1)	2.8369 (5)
Dy(1)–N(2)	2.581 (3)		
Bond angles including Dy(1)			
O(1)–Dy(1)–Br(1)	99.47 (8)	N(1)–Dy(1)–Br(1)	80.59 (8)
O(1)–Dy(1)–O(2)	158.93 (12)	N(2)–Dy(1)–Br(1)	144.52 (8)
O(1)–Dy(1)–N(1)	90.17 (13)	N(2)–Dy(1)–N(1)	64.44 (11)
O(1)–Dy(1)–N(2)	87.00 (12)	N(2)–Dy(1)–N(3)	69.33 (11)

O(1)–Dy(1)–N(3)	76.82 (12)	N(3)–Dy(1)–Br(1)	146.14 (7)
O(1)–Dy(1)–N(4)	90.56 (13)	N(3)–Dy(1)–N(1)	132.48 (11)
O(2)–Dy(1)–Br(1)	101.47 (8)	N(4)–Dy(1)–Br(1)	81.55 (8)
O(2)–Dy(1)–N(1)	95.46 (13)	N(4)–Dy(1)–N(1)	162.00 (11)
O(2)–Dy(1)–N(2)	77.28 (11)	N(4)–Dy(1)–N(2)	133.56 (11)
O(2)–Dy(1)–N(3)	84.48 (12)	N(4)–Dy(1)–N(3)	65.00 (11)
O(2)–Dy(1)–N(4)	90.26 (12)		

3			
Bond lengths around Y(1)			
Y(1)–O(1)	2.1578 (18)	Y(1)–N(3)	2.588 (2)
Y(1)–O(2)	2.1535 (18)	Y(1)–N(4)	2.548 (2)
Y(1)–N(1)	2.578 (2)	Y(1)–Cl(1)	2.6451 (8)
Y(1)–N(2)	2.5834 (19)		
Bond angles including Y(1)			
O1—Y1—Cl1	101.03 (5)	N1—Y1—Cl1	80.61 (5)
O1—Y1—N1	96.00 (7)	N1—Y1—N2	64.64 (6)
O1—Y1—N2	76.77 (6)	N1—Y1—N3	132.64 (6)
O1—Y1—N3	83.91 (7)	N2—Y1—Cl1	144.49 (5)
O1—Y1—N4	90.85 (7)	N2—Y1—N3	69.38 (6)
O2—Y1—Cl1	100.83 (5)	N3—Y1—Cl1	146.12 (5)
O2—Y1—O1	158.02 (7)	N4—Y1—Cl1	81.08 (5)
O2—Y1—N1	89.69 (7)	N4—Y1—N1	161.37 (6)
O2—Y1—N2	86.66 (6)	N4—Y1—N2	133.96 (7)
O2—Y1—N3	76.71 (6)	N4—Y1—N3	65.25 (6)
O2—Y1—N4	90.38 (7)		

4			
Bond lengths around Dy(1)			
Y(1)–O(1)	2.139 (9)	Y(1)–N(3)	2.592(12)
Y(1)–O(2)	2.179 (9)	Y(1)–N(4)	2.600(11)
Y(1)–N(1)	2.593(12)	Y(1)–Br(1)	2.820(3)
Y(1)–N(2)	2.562(11)		
Bond angles including Y(1)			

O1—Y1—Br2	99.5 (3)	N1—Y1—Br2	80.59 (8)
O1—Y1—N1	90.7 (4)	N1—Y1—N4	144.52 (8)
O1—Y1—N2	77.9 (3)	N2—Y1—Br2	64.44 (11)
O1—Y1—N3	87.3 (4)	N2—Y1—N1	69.33 (11)
O1—Y1—N4	90.0 (4)	N2—Y1—N3	146.14 (7)
O1—Y1—O2	158.8 (4)	N2—Y1—N4	132.48 (11)
O2—Y1—Br2	101.6 (3)	N3—Y1—Br2	81.55 (8)
O2—Y1—N1	90.9 (3)	N3—Y1—N1	162.00 (11)
O2—Y1—N2	83.5 (3)	N3—Y1—N4	133.56 (11)
O2—Y1—N3	76.4 (4)	N4—Y1—Br2	65.00 (11)
O2—Y1—N4	95.0 (4)		

Table S3. The calculated results for Dy^{3+} ions configuration by SHAPE 2.0 software for **1** and **2.**

Configuration	**1**	**2**
Heptagon (***D***$_{7h}$)	33.134	33.244
Hexagonal pyramid (***C***$_{6v}$)	23.348	23.491
Pentagonal bipyramid (*D*$_{5h}$)	**1.759**	**2.077**
Capped octahedron (***C***$_{3v}$)	8.040	8.573
Capped trigonal prism (***C***$_{2v}$)	6.289	6.735
Johnson pentagonal bipyramid J13 (***D***$_{5h}$)	2.162	2.263
Johnson elongated triangular pyramid J7 (***C***$_{3v}$)	22.229	22.744

Table S4 Selected bond lengths (Å) and angles (°) for compounds **1**, **2** and the compounds of our previous work (*Inorg. Chem*. **2020**, *59*, 16117−16121).

	1	**1′**		**2**	**2′**
Dy(1)–O(1)	2.156 (2)	2.160 (2)	Dy(1)–O(1)	2.157 (3)	2.155 (2)
Dy(1)–O(2)	2.166 (2)		Dy(1)–O(2)	2.158 (3)	
Dy(1)–N(1)	2.591 (3)	2.568 (3)	Dy(1)–N(1)	2.600 (4)	2.583 (2)
Dy(1)–N(2)	2.591 (3)	2.585 (3)	Dy(1)–N(2)	2.581 (3)	2.578 (2)
Dy(1)–N(3)	2.602 (3)		Dy(1)–N(3)	2.597 (3)	
Dy(1)–N(4)	2.560 (3)		Dy(1)–N(4)	2.566 (4)	
Dy(1)–Cl(1)	2.6576 (10)	2.6680 (14)	Dy(1)–Cl(1)	2.8369 (5)	2.8462 (6)
O(1)–Dy(1)–O(2)	158.09 (9)	156.82 (13)	O(1)–Dy(1)–O(2)	158.93 (12)	157.52 (11)

Table S5. The distances (Å) between neighboring molecules packing along *a*, *b* and *c* directions for **1** and **2**.

Direction of Dy···Dy	**1**	**2**
along ***a*** direction	9.826	9.776
along ***b*** direction	8.640	8.528
along ***c*** direction	10.024	9.884

4. Crystal Structures

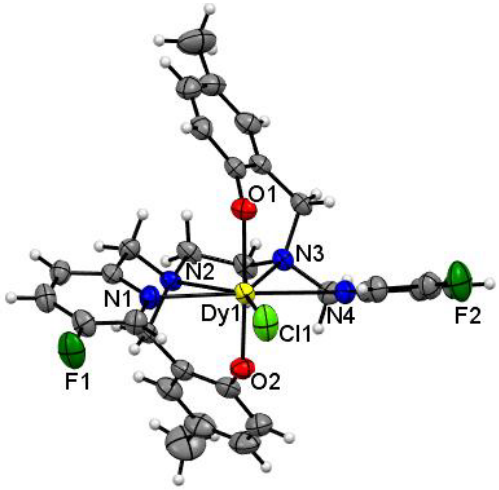

Figure S1. Molecular structure for **2**. Color codes: Dy, yellow; Cl, bright green; O, red; N, blue; C, gray.

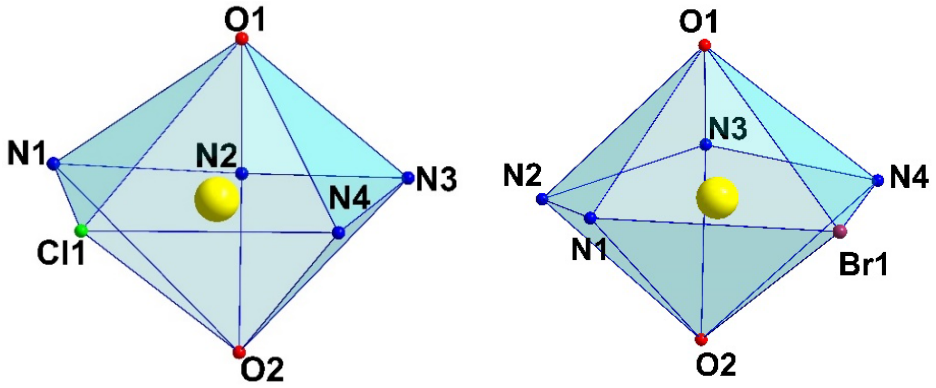

Figure S2. Polyhedrons showing D_{5h} symmetry around Dy^{3+} ion for **1** (left) and **2** (right).

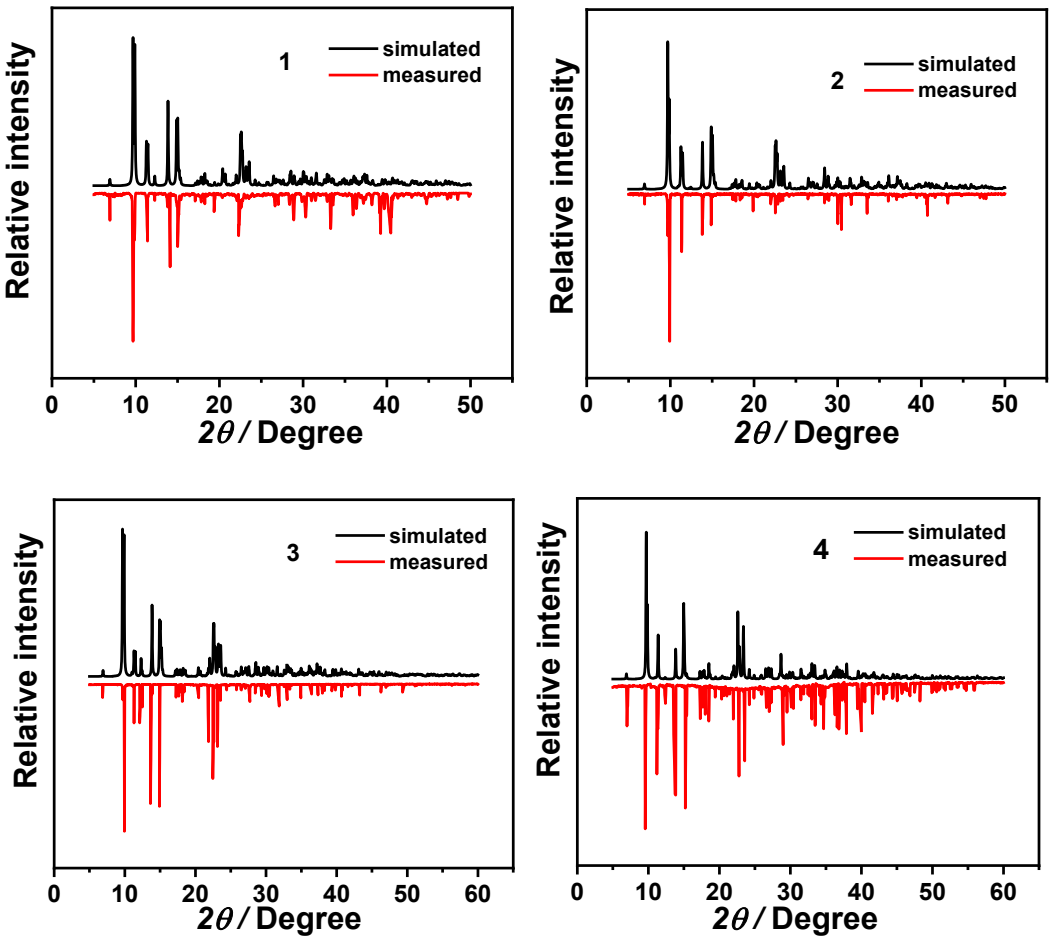

Figure S3. X-ray powder diffraction pattern and simulated PXRD of compounds **1**–**4**.

5. Magnetic Measurements

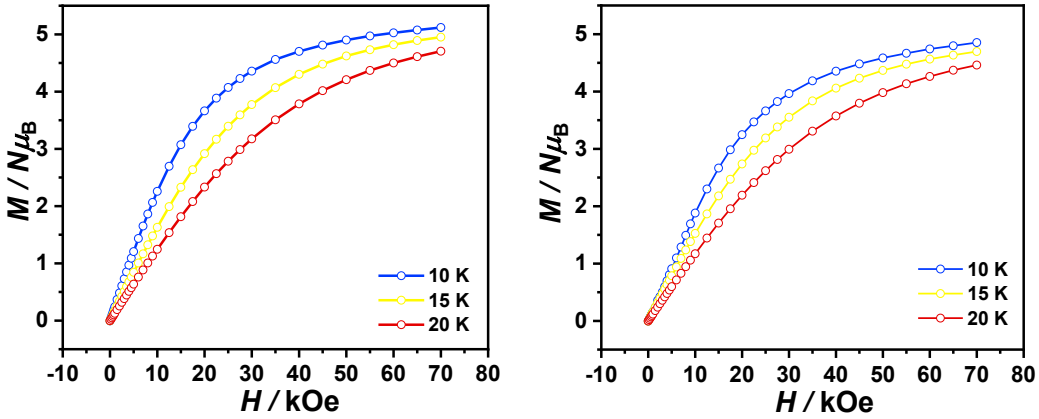

Figure S4. Field dependent magnetization data for complexes **1** (left) and **2** (right) at 2 K. Data were collected from 0 to 70 kOe in steady fields.

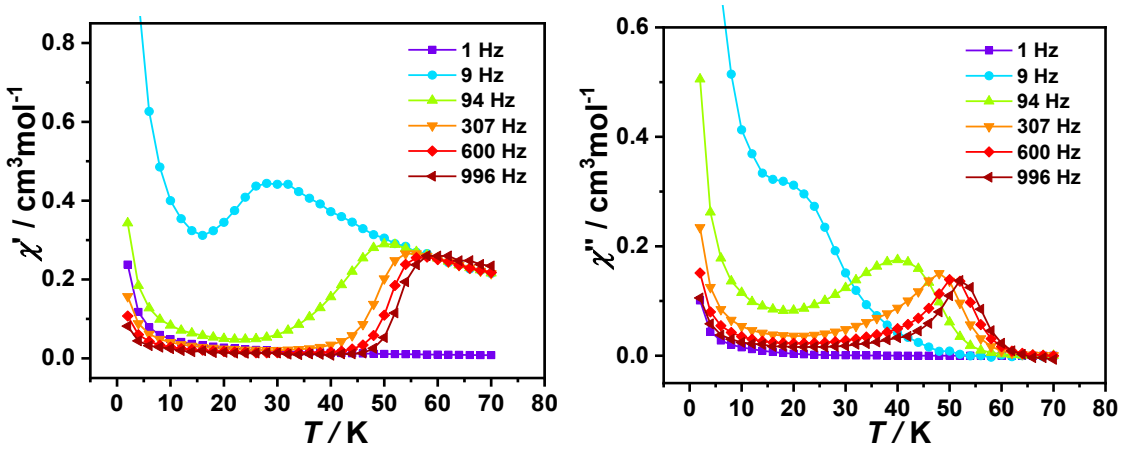

Figure S5. Temperature-dependence of the in-phase component (χ') products in zero dc field for compound **1**.

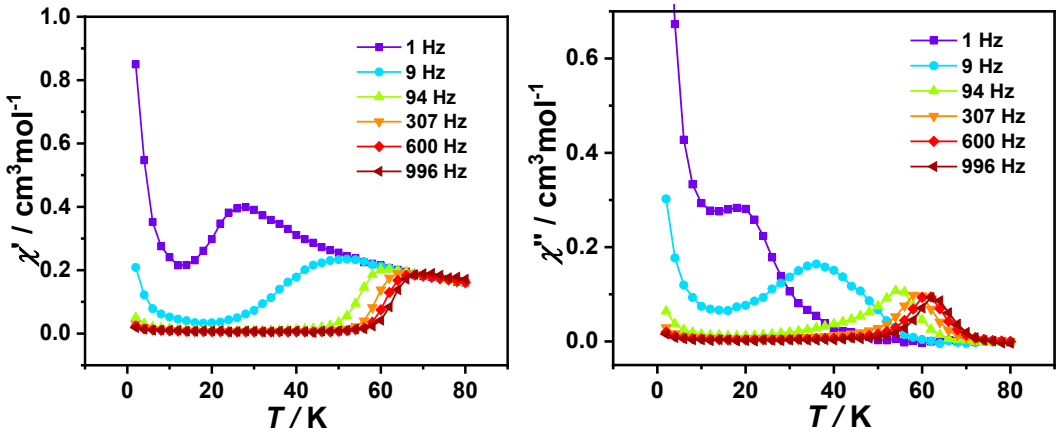

Figure S6. Temperature-dependence of the in-phase component (χ') products in zero dc field for compound **2**.

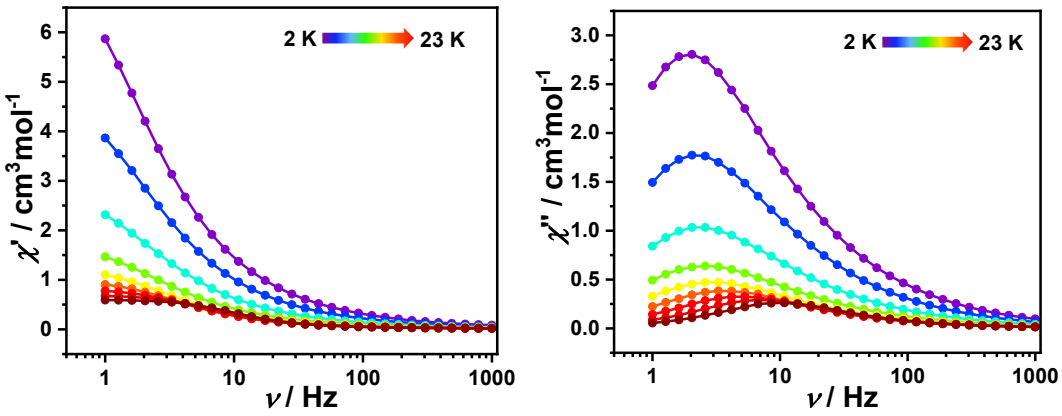

Figure S7. Frequency dependence of in-phase component (χ') and out-of-phase component (χ'') ac susceptibility for **1** in zero applied dc field and at 2–23 K.

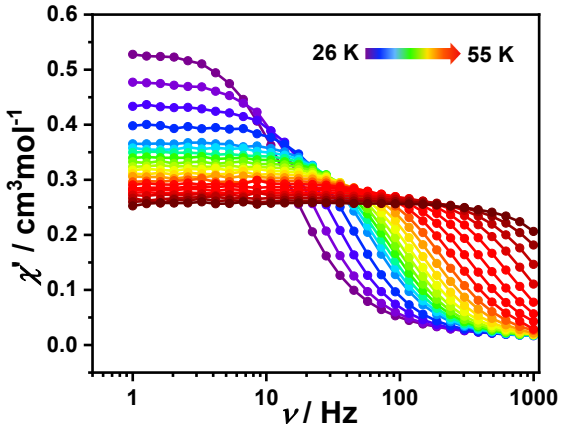

Figure S8. Frequency dependence of in-phase component (χ') ac susceptibility for **1** in zero applied dc field and at indicated temperatures.

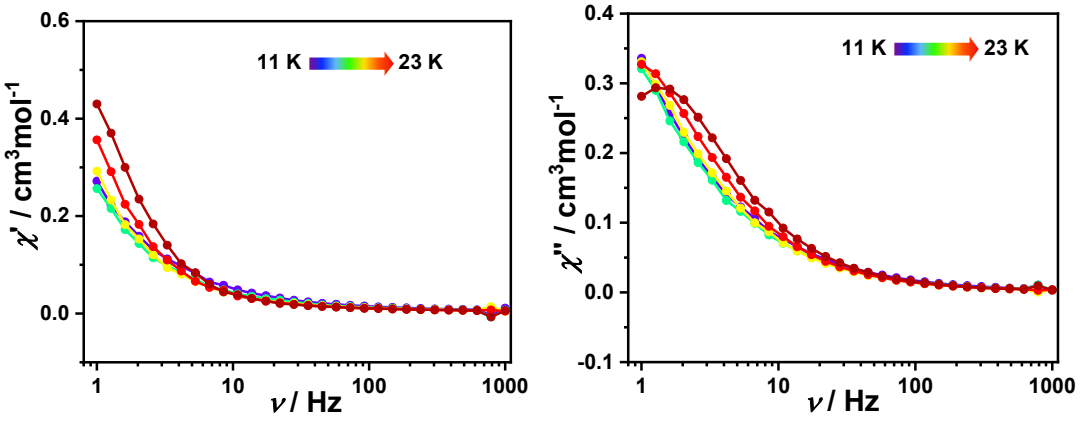

Figure S9. Frequency dependence of in-phase component (χ') and out-of-phase component (χ'') ac susceptibility for **2** in zero applied dc field and at 11–23 K.

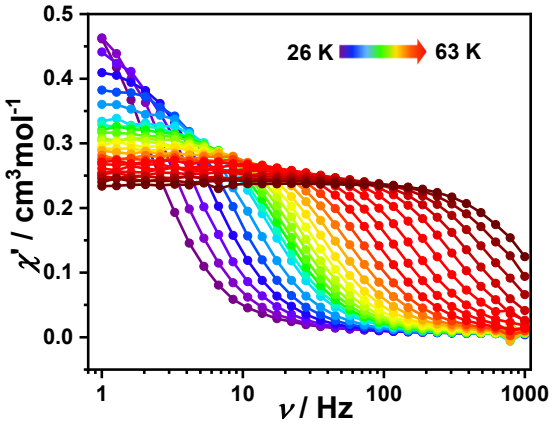

Figure S10. Frequency dependence of in-phase component (χ') ac susceptibility for **2** in zero applied dc field and at 26–63 K.

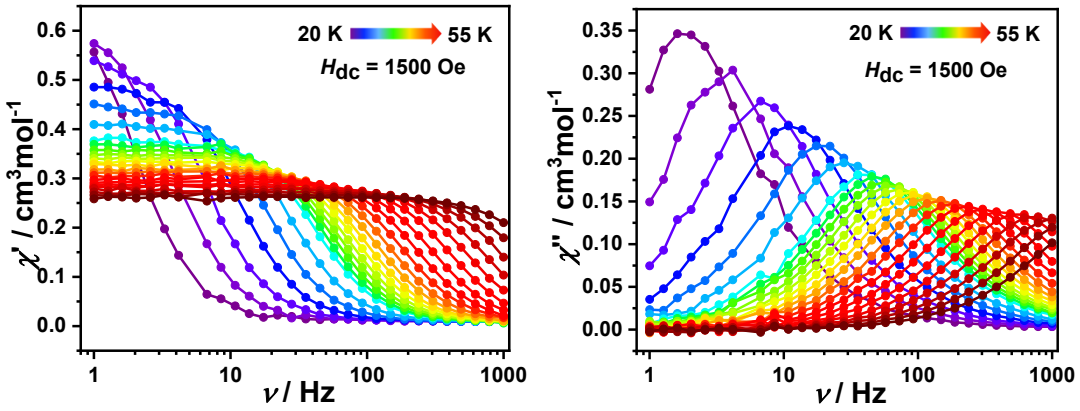

Figure S11. Frequency dependence of in-phase component (χ') and out-of-phase component (χ'') ac susceptibility for **1** in 1500 Oe applied dc field and at 20–55 K.

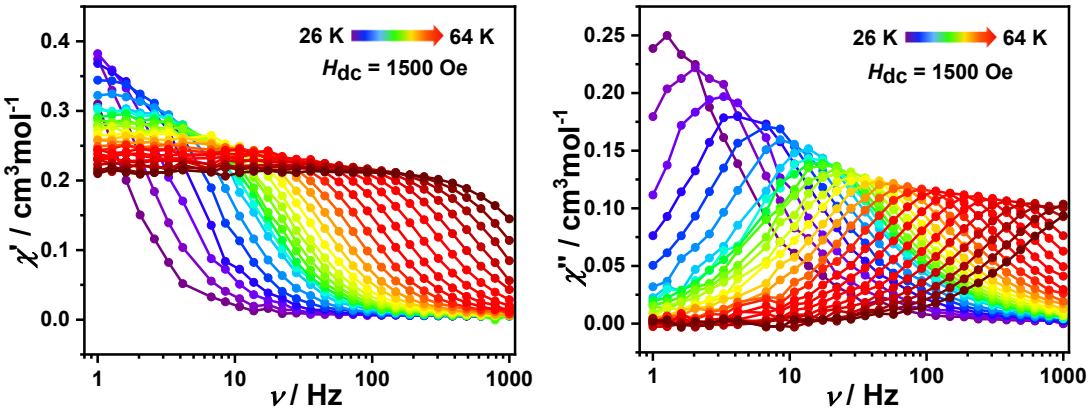

Figure S12. Frequency dependence of in-phase component (χ') and out-of-phase component (χ'') ac susceptibility for **2** in 1500 Oe applied dc field and at 26–64 K.

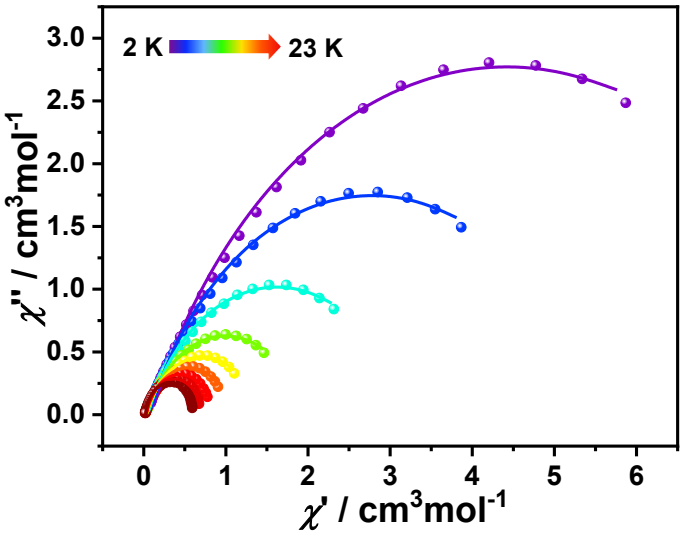

Figure S13. Cole-Cole plots measured at the temperature range of 2−23 K for compound **1**. The best fits to the generalized Debye model specified by solid lines ($0.085 < \alpha < 0.287$).

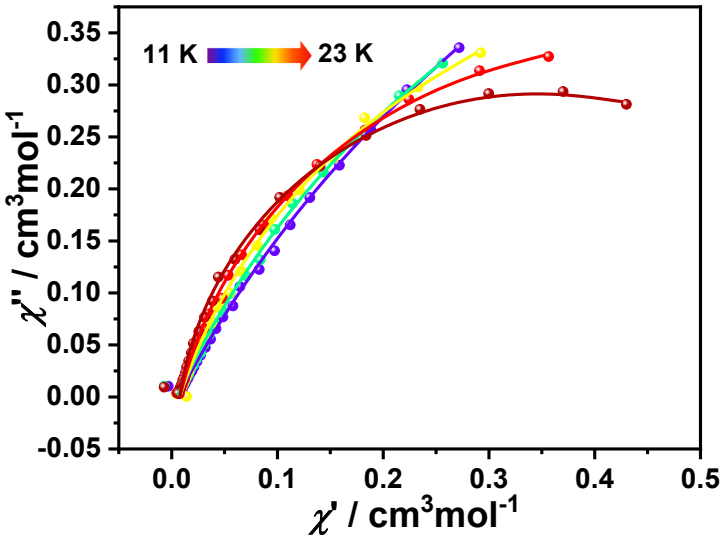

Figure S14. Cole-Cole plots measured at the temperature range of 11−23 K for compound **2**. The best fits to the generalized Debye model specified by solid lines ($0.09 < \alpha < 0.3$).

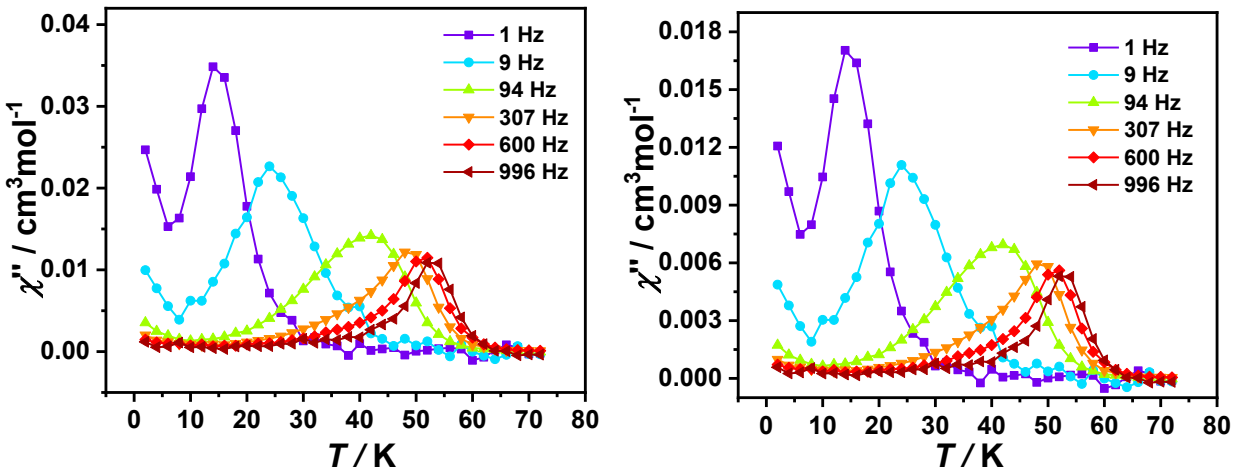

Figure S15. Temperature-dependence of the in-phase component (χ') and out-of-phase component (χ'') products in zero dc field for compound **1@Y**.

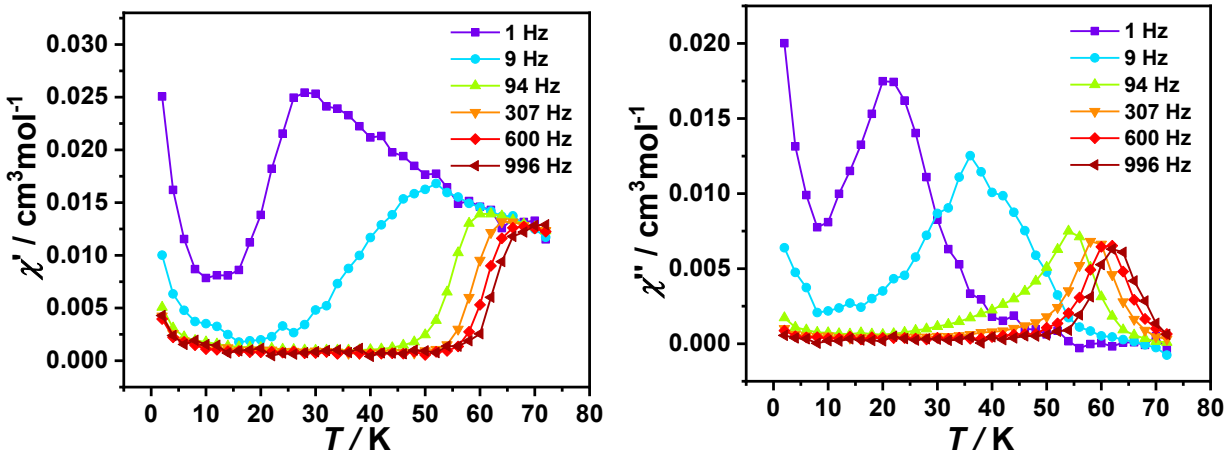

Figure S16. Temperature-dependence of the in-phase component (χ') and out-of-phase component (χ'') products in zero dc field for compound **2@Y**.

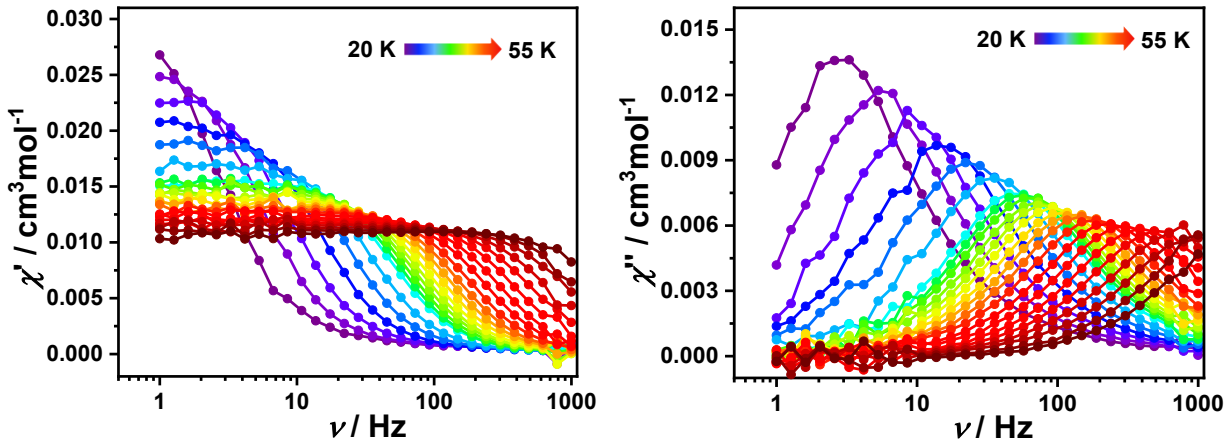

Figure S17. Frequency dependence of in-phase component (χ') and out-of-phase component (χ'') ac susceptibility for **1@Y** in zero applied dc field and at 20–55 K.

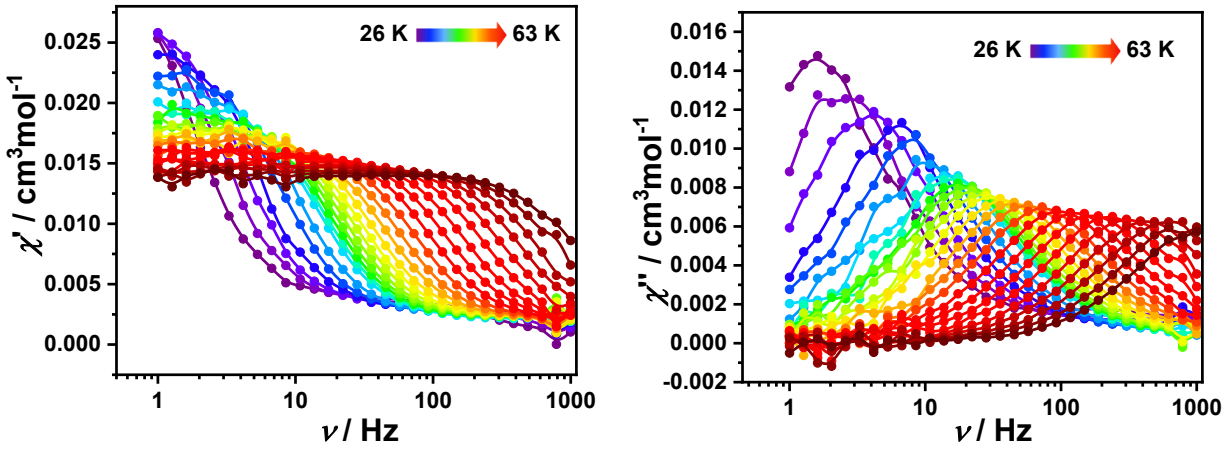

Figure S18. Frequency dependence of in-phase component (χ') and out-of-phase component (χ'') ac susceptibility for **2@Y** in zero applied dc field and at 26–63 K.

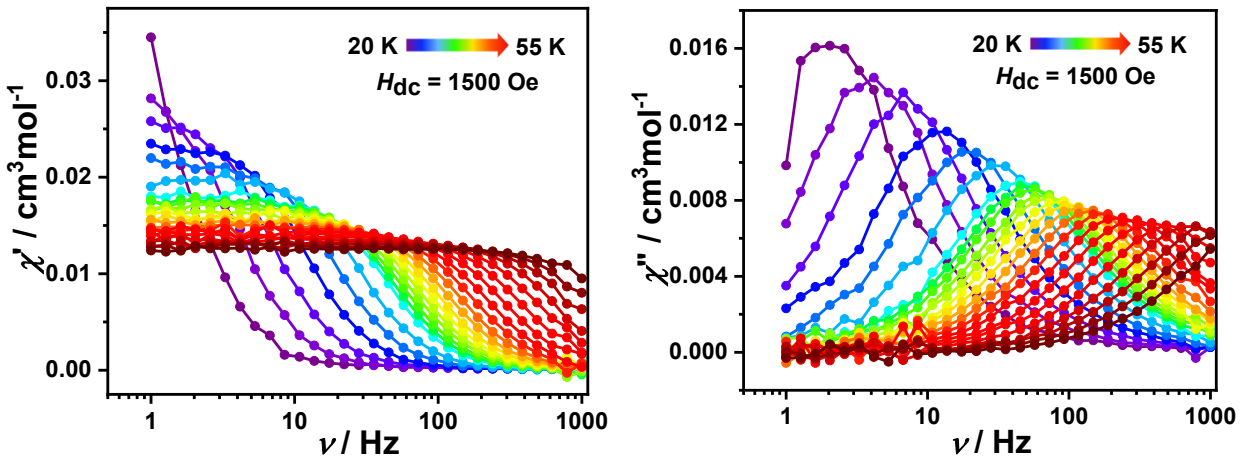

Figure S19. Frequency dependence of in-phase component (χ') and out-of-phase component (χ'') ac susceptibility for **1@Y** in 1500 Oe applied dc field and at 20–55 K.

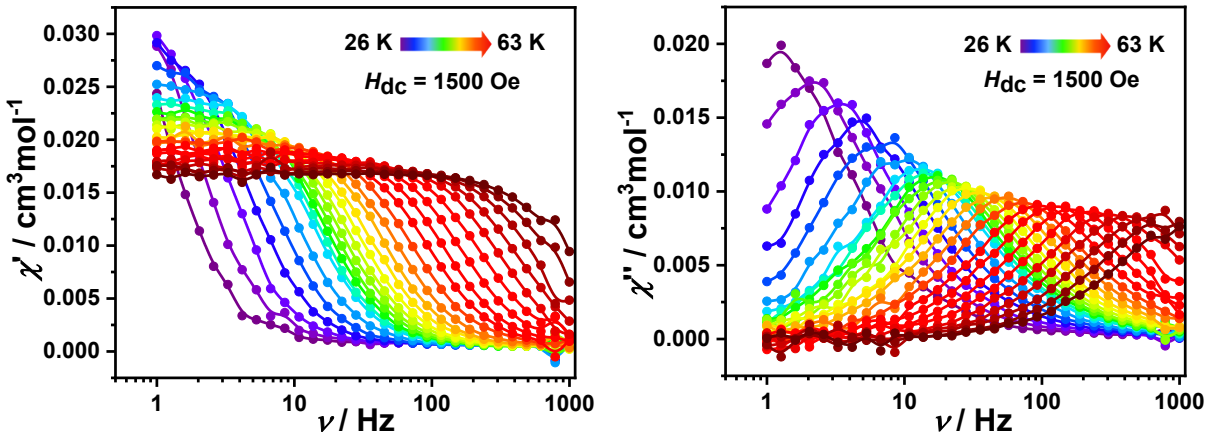

Figure S20. Frequency dependence of in-phase component (χ') and out-of-phase component (χ'') ac susceptibility for **2@Y** in 1500 Oe applied dc field and at 26–63 K.

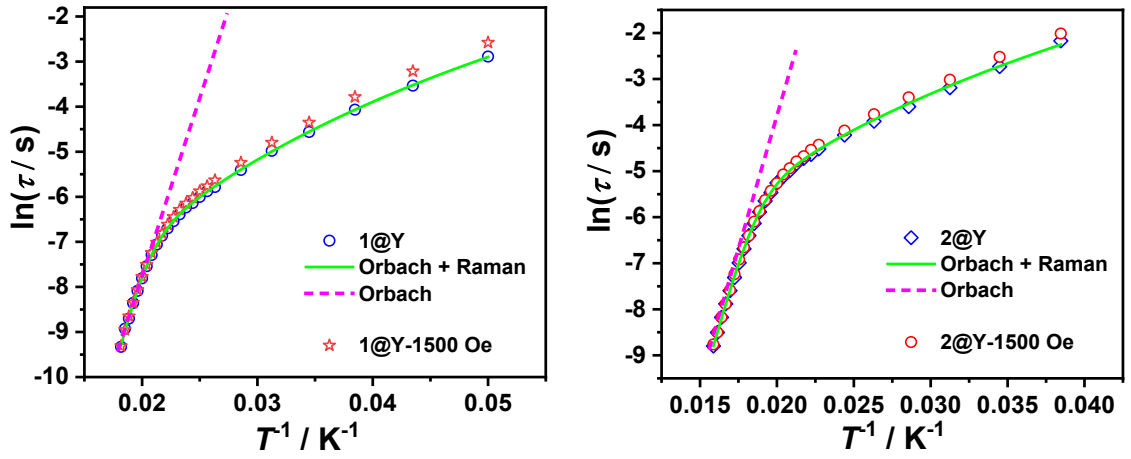

Figure S21. $\ln\tau$ versus T^{-1} plots for **1@Y** (left) and **2@Y** (right) under a 0 Oe and 1500 Oe applied dc field. The magenta dash line represents the part of Orbach process and the green solid line are the best fit for **1@Y** and **2@Y**, see the main text for the fit parameters).

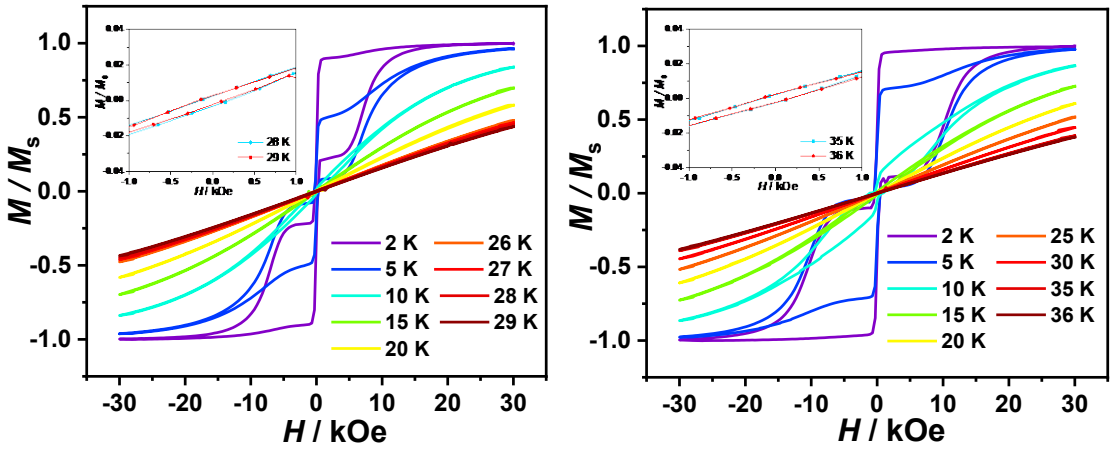

Figure S22. Magnetic hysteresis loop measured at a sweep rate of 200 Oe·s^{-1} for **1@Y** (a) and **2@Y** (b). Insets: Zoomed in hysteresis loop are measured at 28–29 K for **1@Y** and 35–36 K for **2@Y**.

6. Theory Calculations

Multiconfigurational *ab initio* calculations, including spin-orbit coupling (SOC), were performed on the experimental structures of the complexes in this work to explore their SMM properties. This type of calculation includes two steps: 1) a set of spin eigenstates are obtained by the state-averaged (SA) CASSCF method; 2) the low-lying SOC states, i.e., Kramers doublets (KD) herein, are obtained by state interaction which is the diagonalization of the SOC matrix in the space spanned by the spin eigenstates from the first step.

In the CASSCF step, the active space consisted of 9 electrons in 7 orbitals and a total number of 21 sextets were included. Due to the hardware limitation, other highly excited spin states were not considered. The step of state interaction were performed by the RASSI-SO module with the SOC integrals from the AMFI method. The ANO-RCC basis sets, including VTZP for Dy, VDZ for C and H as well as VDZP for other atoms, were used. The SINGLE_ANISO module developed by Chibotaru *et al*, was used to obtain the *g*-tensors, transition magnetic moments and other parameters characterizing the magnetic anisotropy.

Table S6. The relative energies (in cm^{-1}), principal values of g-tensors of the lowest KDs obtained from ab initio calculations

		1	**2**
KD_0	E	0.0000	0.0000
	g_Z	**19.982**	**19.986**
	g_X	1.1025×10^{-03}	4.5992×10^{-04}
	g_Y	1.4937×10^{-03}	6.1608×10^{-04}
	g_{XY}	$\mathbf{1.8565\times10^{-03}}$	$\mathbf{7.6882\times10^{-04}}$
KD_1	E	$4.0538\times10^{+02}$	$4.1843\times10^{+02}$
	g_Z	$1.6994\times10^{+01}$	$1.7049\times10^{+01}$
	g_X	1.0788×10^{-01}	6.3817×10^{-02}
	g_Y	1.4926×10^{-01}	7.6189×10^{-02}
	g_{XY}	1.8416×10^{-01}	9.9385×10^{-02}
KD_2	E	$6.4611\times10^{+02}$	$6.8981\times10^{+02}$
	g_Z	$1.1876\times10^{+01}$	$1.3760\times10^{+01}$
	g_X	$2.0815\times10^{+00}$	7.3990×10^{-01}

	g_Y	$4.6897\times10^{+00}$	$1.2378\times10^{+00}$
	g_{XY}	$5.1309\times10^{+00}$	$1.4421\times10^{+00}$
KD_3	E	$7.3066\times10^{+02}$	$8.1058\times10^{+02}$
	g_Z	$9.4966\times10^{+00}$	$1.0555\times10^{+01}$
	g_X	$6.1284\times10^{+00}$	$4.5806\times10^{+00}$
	g_Y	$1.4758\times10^{+00}$	$5.2911\times10^{+00}$
	g_{XY}	$6.3035\times10^{+00}$	$6.9985\times10^{+00}$
KD_4	E	$8.1763\times10^{+02}$	$8.7154\times10^{+02}$
	g_Z	$1.0259\times10^{+01}$	$8.4665\times10^{+00}$
	g_X	1.9363×10^{-01}	$5.4878\times10^{+00}$
	g_Y	$3.7539\times10^{+00}$	3.6774×10^{-01}
	g_{XY}	$3.7589\times10^{+00}$	$5.5001\times10^{+00}$
KD_5	E	$8.4069\times10^{+02}$	$8.9189\times10^{+02}$
	g_Z	$1.3561\times10^{+01}$	$1.0718\times10^{+01}$
	g_X	$1.4448\times10^{+00}$	6.5488×10^{-01}
	g_Y	$4.5730\times10^{+00}$	$1.0041\times10^{+00}$
	g_{XY}	$4.7958\times10^{+00}$	$1.1988\times10^{+00}$
KD_6	E	$8.6643\times10^{+02}$	$9.0455\times10^{+02}$
	g_Z	$1.7035\times10^{+01}$	$1.1780\times10^{+01}$
	g_X	1.3742×10^{-01}	8.7221×10^{-02}
	g_Y	$1.0790\times10^{+00}$	$5.3177\times10^{+00}$
	g_{XY}	$1.0878\times10^{+00}$	$5.3184\times10^{+00}$
KD_7	E	$9.2646\times10^{+02}$	$9.6104\times10^{+02}$
	g_Z	$1.8224\times10^{+01}$	$1.6845\times10^{+01}$
	g_X	2.4306×10^{-01}	6.6038×10^{-01}
	g_Y	3.3850×10^{-01}	$1.6153\times10^{+00}$
	g_{XY}	4.1672×10^{-01}	$1.7451\times10^{+00}$